Structures of maltohexaose and maltoheptaose bound at the donor sites of cyclodextrin glycosyltransferase give insight into the mechanisms of transglycosylation activity and cyclodextrin size specificity

Uitdehaag, JCM; van Alebeek, GJWM; Dijkhuizen, L; Dijkstra, BW; Alebeek, Gert-Jan W.M. van; Dijkstra, Bauke W.

Published in:
Biochemistry

DOI:
10.1021/bi000340x

Publication date:
2000

Structures of Maltohexaose and Maltoheptaose Bound at the Donor Sites of Cyclodextrin Glycosyltransferase Give Insight into the Mechanisms of Transglycosylation Activity and Cyclodextrin Size Specificity[†,‡]

Joost C. M. Uitdehaag,[§] Gert-Jan W. M. van Alebeek,[||] Bart A. van der Veen,[||] Lubbert Dijkhuizen,[||] and Bauke W. Dijkstra*[,§]

Center for Carbohydrate Bioengineering and Laboratory of Biophysical Chemistry, University of Groningen, Nijenborgh 4, 9747 AG Groningen, The Netherlands, and Center for Carbohydrate Bioengineering and Department of Microbiology, University of Groningen, Kerklaan 30, 9751 NN Haren, The Netherlands

Received February 14, 2000

ABSTRACT: The enzymes from the α-amylase family all share a similar α-retaining catalytic mechanism but can have different reaction and product specificities. One family member, cyclodextrin glycosyltransferase (CGTase), has an uncommonly high transglycosylation activity and is able to form cyclodextrins. We have determined the 2.0 and 2.5 Å X-ray structures of E257A/D229A CGTase in complex with maltoheptaose and maltohexaose. Both sugars are bound at the donor subsites of the active site and the acceptor subsites are empty. These structures mimic a reaction stage in which a covalent enzyme−sugar intermediate awaits binding of an acceptor molecule. Comparison of these structures with CGTase−substrate and CGTase−product complexes reveals three different conformational states for the CGTase active site that are characterized by different orientations of the centrally located residue Tyr 195. In the maltoheptaose and maltohexaose-complexed conformation, CGTase hinders binding of an acceptor sugar at subsite +1, which suggests an induced-fit mechanism that could explain the transglycosylation activity of CGTase. In addition, the maltoheptaose and maltohexaose complexes give insight into the cyclodextrin size specificity of CGTases, since they precede α-cyclodextrin (six glucoses) and *β*-cyclodextrin (seven glucoses) formation, respectively. Both ligands show conformational differences at specific sugar binding subsites, suggesting that these determine cyclodextrin product size specificity, which is confirmed by site-directed mutagenesis experiments.

The α-amylase family, or glycosyl hydrolase family 13 (*1*), is a large and well-studied family of enzymes (for reviews see refs *2*−*4*). Some well-known family 13 enzymes are α-amylase, isoamylase, neopullulanase, and cyclodextrin glycosyltransferase (CGTase).[1] All these enzymes share a similar catalytic site architecture (*2, 5*) and use a similar α-retaining mechanism to process their substrates (*6, 7*). On the other hand, the α-amylase family enzymes exhibit a wide range of product specificities, making them useful tools in the industrial processing of starch (*8, 9*).

Product specificity is conferred by sugar binding subsites near the catalytic subsite, which is illustrated for the enzyme CGTase in Figure 1. CGTase, as most family 13 enzymes, binds its substrate, starch, across multiple sugar binding subsites (labeled −7 to +2) (*10*). In the first step of catalysis, an α(1→4) glycosidic bond is cleaved between subsites −1 and +1, leading to an intermediate that is covalently linked to Asp 229 at subsite −1. The sugar chain of the covalent intermediate is called donor sugar and is bound at the donor subsites (−1 to −7). In the next reaction step, the leaving group is expelled from the other subsites (+1 and +2) and replaced by an acceptor molecule, hence subsites +1 and +2 are called acceptor sites. In the final reaction step, a new α(1→4) glycosidic bond is formed between the donor and acceptor to form a product (Figure 1).

On the basis of this reaction scheme, two types of product specificity can be distinguished, acceptor and donor types. CGTase clearly has acceptor specificity since it can use a water molecule as acceptor in an hydrolysis reaction but has ∼100 times higher activity when it uses free sugars (typically maltose) as acceptor in a transglycosylation, or disproportionation, reaction (*11*) (Figure 1). Thus, CGTase is a transferase, in contrast to most α-amylases, which are hydrolases (*3*). Most characteristically, CGTase can catalyze an intramolecular transglycosylation (cyclization) reaction using the sugar at the nonreducing end of the covalent intermediate as acceptor, leading to a circular product, a cyclodextrin (*12*) (Figure 1).

The donor specificity of CGTase determines the preferred sugar chain length that is bound at the donor sites and thereby

[†] Work at the ELETTRA synchrotron Trieste was sponsored by EU Grant ERB FMGE CT950022. Work at the EMBL outstation Hamburg was sponsored by EU Grant ERB FMGE CT980134.

[‡] Coordinates for the complexes of E257A/D229A CGTase with maltoheptaose and maltohexaose have been deposited with the Brookhaven Protein Data Bank (ID codes 1EO5 and 1EO7, respectively).

* Corresponding author: Telephone +31-50-3634381; fax +31-50-3634800, e-mail bauke@chem.rug.nl.

[§] Laboratory of Biophysical Chemistry.

[||] Department of Microbiology.

[1] Abbrevations: G6, maltohexaose; G7, maltoheptaose; G9, maltononaose; CGTase, cyclodextrin glycosyltransferase; CD, cyclodextrin; BC251, *Bacillus circulan*s strain 251.

10.1021/bi000340x CCC: $19.00
Published on Web 06/03/2000

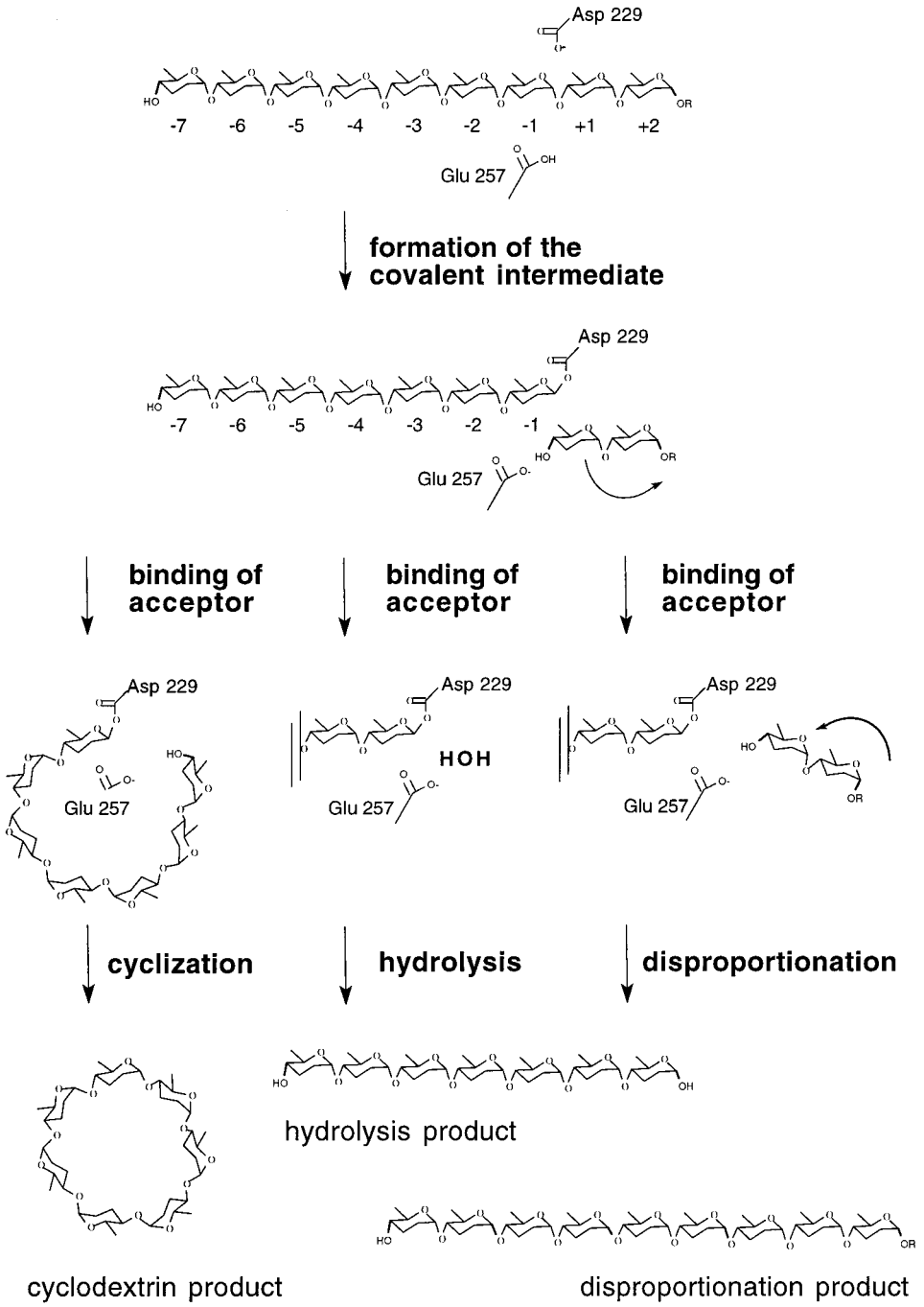

FIGURE 1: Overview of the catalytic cycle of CGTase. After substrate binding (top) an α(1→4) glycosidic bond in the substrate is broken, leading to a β(1→4) glycosidically linked covalent intermediate (top). Then an acceptor molecule is bound, which can be the nonreducing end of the covalently bound intermediate, a water molecule, or another linear maltooligosaccharide. The acceptor molecule subsequently attacks the −1 glucose C1 atom leading to a cyclodextrin product (cyclization), a linear hydrolysis product, or a longer linear oligosaccharide (transglycosylation or disproportionation). Where appropriate, the linear sugar chain is condensed by double bars. CGTase can also degrade cyclodextrins (coupling activity), which is sometimes considered as a fourth reaction type. It is the reverse of the cyclization reaction.

the size of cyclodextrin that is predominantly formed (*13*) (Figure 1). Cyclodextrins comprise typically six, seven, or eight glucoses (α-, β-, or γ-cyclodextrin respectively), but larger ones are also produced (*14*). Depending on the bacterial source of CGTase, strong size specificities have been reported (*15*). In addition, many attempts were made to improve the size specificity of industrially used CGTases through site-directed mutagenesis (*13, 16, 17*).

To study the acceptor (transglycosylation) and donor (cyclodextrin size) type specificities in CGTase, we have determined the structures of maltohexaose (G6) and maltoheptaose (G7) bound to the catalytically inactive E257A/D229A mutant of the CGTase from *B. circulans* strain 251. These linear oligosaccharides bind from subsites −1 to −6 and from −1 to −7, respectively. The differences in binding of these sugars at the donor subsites elucidate the atomic basis of α/β-cyclodextrin size specificity. Furthermore, both structures provide a unique view of the CGTase conformation after leaving group departure and prior to acceptor binding. Comparison with X-ray structures of CGTase substrate and

product complexes and the analysis of structural rearrangements allows a deeper insight into the molecular mechanisms of the enzyme's transglycosylation specificity.

EXPERIMENTAL PROCEDURES

Mutagenesis and Crystal Soaking. Crystals of the *Bacillus circulans* strain 251 (BC251) CGTase have proven to be an excellent experimental system for determining 3D structures of CGTase−ligand complexes (*7, 10, 12, 18*). In these crystals, natural substrates can be processed by CGTase, even when a E257Q/D229N mutant with a 700 000-fold reduced activity is used (*7, 18*). With this mutant, soaking of CGTase crystals in a maltoheptaose (G7) solution always resulted in electron density for a maltononaose (G9) (unpublished result). This presumably results from a transglycosylation reaction with maltose as acceptor, since maltose is present in the crystallization setups (*19*).

To prevent this transglycosylation, we constructed a *B. circulans* strain 251 E257A/D229A mutant CGTase. Mutagenesis was performed with PCR as described earlier and verified by sequencing (*13*). Expression and purification was done in a standard way (*13*). An activity assay indicated a >1000-fold reduced activity in comparison with E257Q/D229N CGTase. The E257A/D229A CGTase mutant was crystallized from 60% (v/v) MPD (2-methyl-2,4-pentanediol), 100 mM Tris buffer, pH 8.1, and 5% (w/v) maltose, similar to the crystallization conditions of wild-type CGTase (*19*).

To further minimize unwanted transglycosylation activity in these crystals, we replaced all the maltose in the crystals by 4-deoxymaltose, which is incompetent as acceptor (*20*). The crystals were washed for 10 min in maltose-free mother liquor and subsequently transferred for 10 h to fresh mother liquor containing 5% (w/v) 4-deoxymaltose. This procedure was repeated four times. Directly before soaking with maltoheptaose and maltohexaose, the crystals were washed in a mother liquor containing no sugars, 60% (v/v) MPD, and 100 mM MES [2-(*N*-morpholino)ethanesulfonic acid] buffer at pH 6.1, which is close to the optimum pH of wild-type CGTase (*18*). One crystal was subsequently soaked in the mother liquor containing 10 mg/mL maltoheptaose and after 40 min was frozen to 100 K under a cold nitrogen stream for data collection. Another crystal was soaked in the mother liquor containing 10 mg/mL maltohexaose and after 30 min was frozen to 120 K.

Refinement of the CGTase−Maltoheptaose Complex. Data for the maltoheptaose complex were collected to 2.0 Å at the EMBL beamline X11 of DESY, Hamburg, Germany. Processing was done with DENZO/Scalepack (*21*). The E257Q/D229N CGTase−maltotetraose complex at 120 K (*18*), with all sugars and water molecules removed, was used as a starting model. Refinement was done with TNT (*22*) in a standard way (*18*). Sugar ligands were manually placed in σ_A-weighted (*23*) $2F_o - F_c$, $F_o - F_c$, and OMIT $2F_o - F_c$ electron density maps (*24*) with the program O (*25*). It appeared that a G7 ligand had bound from subsites −1 to −7, with the glucose at subsite −1 in its β-anomeric configuration. At subsite +1, an MPD molecule was observed, but no sugars were bound at the acceptor sites. Furthermore, various ligands were bound at the three maltose binding sites that are present in the noncatalytic domains of CGTase (*19*) (Table 1).

Table 1: Data and Model Statistics of the BC251 E257A/D229A CGTase Complexes

	ligands	
	maltoheptaose (G7)	maltohexaose (G6)
Data Collection		
space group	$P2_12_12_1$	$P2_12_12_1$
cell axes *a, b, c* (Å)	67.5, 109.7, 116.7	64.7, 109.0, 111.6
resolution range (Å)	79.9−2.00	78.0−2.48
no. of unique reflections	54 766	26 146
R_{merge}[a] (%) and $\langle I/\sigma \rangle$	11.1, 7.7	6.1, 14.4
completeness (%)	92.1	91.2
Statistics of the Last Resolution Shell		
R_{merge}[a] (%) and $\langle I/\sigma \rangle$	41.4, 2.9	22.5, 4.2
completeness (%)	88.1	86.4
Refinement Statistics		
no. of amino acids	686 (all)	686 (all)
no. of Ca^{2+} atoms	3	3
no. of MPD molecules	1	0
active-site ligand	maltoheptaose	maltohexaose
MBS1 ligand[b]	maltotetraose	maltotriose
MBS2 ligand[b]	maltotetraose	maltotetraose
MBS3 ligand[b]	maltotriose	maltotriose
no. of solvent sites	674	145
average *B* factor (Å^2)	19.1	42.7
final *R* factor[c] (%)	16.7	22.8
final free *R* factor[d] (%)	21.0	29.6
Rms Deviation from Ideal Geometry		
bond lengths (Å)	0.006	0.006
van der Waals contacts (Å)	0.010	0.012
B factor correlations (Å^2)	1.4	1.0

[a] $R_{merge} = \sum_h \sum_i |I(h) - I_i(h)| / \sum_h \sum_i I_i(h)$, where reflection *h* has intensity $I_i(h)$ on occurrence *i* and mean intensity $I(h)$. $\langle I/\sigma \rangle$ is the average ratio of intensity and standard deviation of all reflections *h* after averaging over their occurrences *i*. [b] MBS1−3 indicate the three maltose binding sites near residues Trp616/Trp662, Leu600/Tyr633, and Trp413 (*19*). Ligands there might represent G6 and G7 that are partially visible. [c] *R* factor $= \sum_h |F_o - F_c| / \sum_h F_o$, where F_o and F_c are the observed and calculated structure factor amplitudes of reflection *h*, respectively. [d] The free *R* factor is calculated as the *R* factor with F_o that were excluded from the refinement (5% of the data).

Ideal bond lengths and angles for the sugar ligands were obtained from the crystal structures of maltose and cellobiose (*26*). For MPD, they were obtained from the USF hetero compounds database at www.alpha2.bmc.uu.se/hicup. In the last stages of refinement, explicit solvent molecules were included by use of BIOMOL software (available at www.xray.chem.rug.nl/software.html). The stereochemistry of the complete model was checked with WHATCHECK (*27*). The final electron density for the ligands in the active site is shown in Figure 2A. Model and data statistics are given in Table 1.

Refinement of the CGTase−Maltohexaose Complex. Data for the maltohexaose complex were collected to 2.48 Å at the protein crystallography beamline of the ELETTRA synchrotron near Trieste and processed as the CGTase−maltoheptaose data. Surprisingly, the longest cell axis, which normally measures about 117 Å, had changed to 111 Å (Table 1). Presumably for this reason, initial rigid-body refinement failed. Therefore, we performed a molecular replacement search with AMoRe (*28*), using the protein coordinates of the BC251 E257Q CGTase−intermediate complex (*7*) as search model, since this structure has the most similar cell axes. The best solution was refined as described above. The electron density shows the presence of a maltohexaose ligand in the active site, bound from

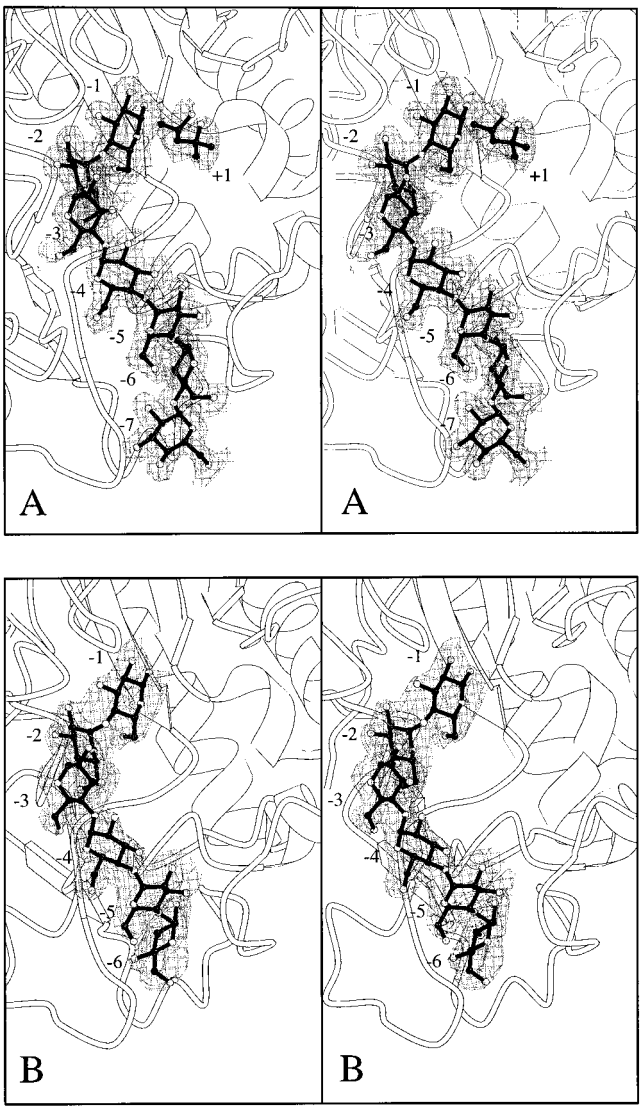

FIGURE 2: Stereopictures of the final electron density for the ligands bound to BC251 E257A/D229A CGTase. The σ_A (*23*) weighted $2F_o - F_c$ OMIT (*24*) electron density is contoured at 0.8 times its standard deviation. (A) Maltoheptaose (G7) bound from subsites −1 to −7 and MPD at subsite +1. (B) Maltohexaose (G6) bound from sites −1 to −6. This figure and Figures 4 and 5 were made with Bobscript (*37*).

subsites −1 to −6 (Figure 2B). At subsite −1, a glucose β-anomer was modeled in analogy with the CGTase−maltoheptaose complex. No ligand is bound at subsite +1 or +2, but various ligands are observed at the maltose binding sites (Table 1).

The electron density showed that the compression of the longest cell axis is due to a more compact crystal packing at the maltose binding site near Tyr 633 and Leu 600. Presumably, this is correlated to rearrangements in the CGTase backbone after binding of the maltohexaose (see below). The adaptation of crystal packing after ligand binding has affected the crystal quality, as shown by the reduced resolution of the data and the high overall *B*-factor of the structure (Table 1).

RESULTS

The structures of BC251 E257A/D229A CGTase complexed with maltoheptaose (G7) and maltohexaose (G6) show

Table 2: Interactions of G6 and G7 with BC251 E257A/D229A CGTase

atoms offering contacts in CGTase	distances (Å) and the glucose atom making the contact	
	maltoheptaose	maltohexaose
subsite +2	empty	empty
subsite +1	MPD[a]	empty
subsites −1 and −2[b]		
subsite −3		
Asn 94 Oδ1/Thr 95 O/ Tyr 97 Oη/His 98 Nϵ/ Asp 371 Oδ1	dwm[c] to O6 and O5	
Asp 196 Oδ1		wm[d] to O6
Asp 371 Oδ2	3.1 O2[e]	2.8 O2[e]
subsite −4		
glucose atom O3 at site −3	2.7 O2	2.7 O2
subsite −5		
Thr 181 O and Tyr 195 N	wm[d] to O3	wm[d] O3
glucose atom O2 at site −4	2.9 O3	3.2 O3
subsite −6		
Ser 145 Oγ		3.1 O4
Asn 193 Nδ	3.1 O2	3.1 O2 and 3.1 O3
Tyr 195 O	2.7 O2	2.7 O2
Asp 196 O/Ala 144 O	wm[d] to O2 and O3	
Gly 179 N/Tyr 167 Oη	wm[d] to O3	
Gly 180 N	wm[d] to O5 and O6	
subsite −7		empty
Ser 145 Oγ	2.9 O3	
Asp 147 N	2.9 O3	
Asp 147 Oδ1	2.8 O4[e]	
glucose atom O3 at −6	3.0 O2	
symm.-rel. Tyr 456 Oη	wm[d] to O6	

[a] Hydrophobic interactions only. [b] Binding contacts were identical to those in the CGTase−maltotriosyl covalent intermediate complex (*7*); see text. [c] Mediated by two waters. [d] Mediated by one water. [e] This contact has a close distance but bad hydrogen-bond geometry.

that these compounds bind in the active site from subsites −1 to −7 and −1 to −6, respectively, and are well-defined (Figure 2). An overview of all interactions is given in Table 2 and Figure 3. Comparing these new structures with those of previously determined stable states along the reaction coordinate (*7*, *12*) gives insight into the mechanisms of catalysis and specificity of CGTase. However, such comparisons need to exclude artifacts arising from experimental differences in pH and mutations. Therefore we compared the structures of unliganded E257A/D229A BC251 CGTase at pH 6.1 and 10.3 with that of E257Q/D229N BC251 CGTase at pH 10.3. No differences exceeding the coordinate error in the structures (∼0.2 Å) were observed. Below, the high-resolution CGTase−G7 complex is compared with the structures of other reaction states (Figure 4). Subsequently, the differences between the G7 and G6 complexes are described (Figure 5).

Maltoheptaose Mimics the Covalent Intermediate at Subsite −1. The reducing-end glucose of G7 binds in the catalytic subsite −1 in the β-anomeric state, with its ring positioned deep into the active-site cleft in an undistorted $^4C_1$ chair conformation (Figures 3A and 4A). The position of the glucose ring in subsite −1 superimposes best with the glucose in a CGTase−covalent intermediate complex (*7*) (Figure 4B). This position is allowed by the mutation Asp 229 Ala, in the absence of which a 2.0 Å van der Waals contact between the Asp 229 Oδ1 atom and the glucose C1 atom would occur. A similar ring orientation for a β-anomeric glucose at subsite −1 was observed in a *B. circulans*

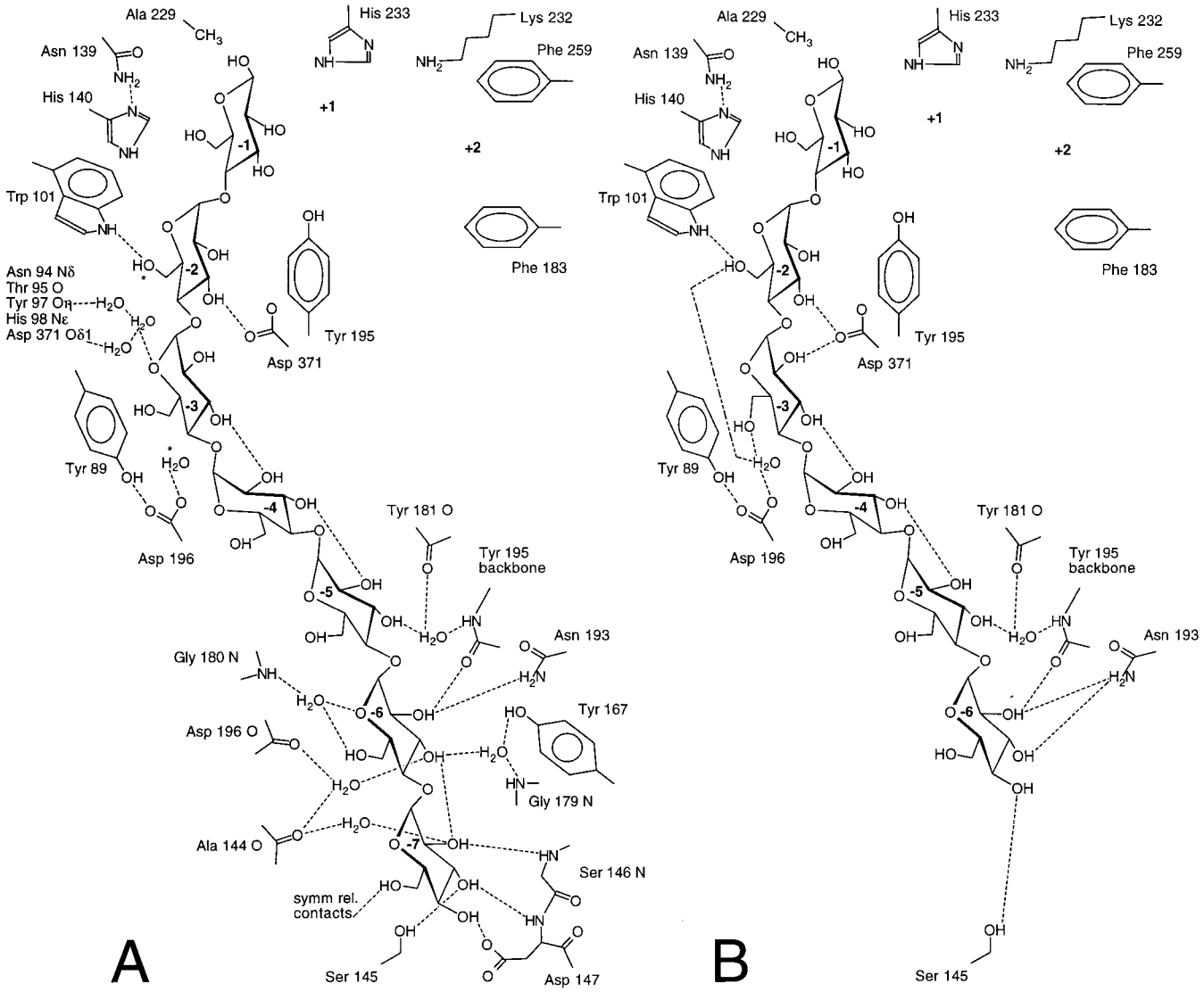

FIGURE 3: Scheme of all interactions of (**A**) maltoheptaose (G7) and (**B**) maltohexaose (G6) with BC251 E257A/D229A CGTase. Dashed lines indicate interactions for which the distances are given in Table 2. In one case, asterisks (*) near interacting atoms replace a dashed line. For clarity, some interactions at subsites −1 (involving Tyr 100, Arg 227, His 327, and Asp 328) and −2 (His 98 and Arg 375) have been omitted in this figure. Within the error limits of our structures, these interactions are identical to those in the CGTase-covalent intermediate complex (*7*). The residues comprising subsites +1 and +2 have been incorporated for clarity. Due to its limited resolution, fewer water-mediated interactions are visible in the G6 structure than in the G7 structure.

strain 8 D229A CGTase−maltotriose complex (*16*). The interactions of the G7 ligand at subsite −1 are similar to those in the CGTase−covalent intermediate complex, including hydrophobic stacking to Tyr 100, absence of a hydrogen bond between the sugar OH-6 group and His 140, and the presence of a hydrogen bond between the O1 atom and Arg 227 (*7*). This latter contact stabilizes the β-anomeric configuration of the C1−O1 bond in the catalytic site, which mimics the β-glycosidic bond between the C1 atom and the Asp 229 Oδ1 atom in the intermediate (*7*) (Figure 4B). Thus the binding mode of maltoheptaose at subsite −1 resembles that of the covalent intermediate.

Maltoheptaose and Maltononaose Binding Modes Differ at Subsite −3. In previous work, we reported the structure of a maltononaose (G9) linear substrate bound to BC251 CGTase from subsites −7 to +2 (*7*). When the binding mode of G7 is compared to this G9 structure, both sugar chains superimpose well at subsites −2 and subsites −4 to −7, but surprisingly, differences appear at subsite −3. The G7 sugar at subsite −3 has shifted 1.8 Å out of the cleft formed by Tyr 89 and Tyr 195 compared to the G9 sugar, thereby losing the ability to interact with Asp 196 (Figure 4C). Furthermore, the G7 structure has a different conformation of the flexible loop comprising residues 87−93, which is part of subsite −3 (Figure 4C). The 87−93 loop conformation in the G7 complex resembles that observed in unliganded and γ-cyclodextrin-liganded CGTase (*12*). These differences at subsite −3 likely originate from the fact that in the G7 complex no acceptor sugar has bound, whereas such a sugar is present in the G9 structure (Figure 4A; see below).

Maltoheptaose Binding Mode at Subsite −3 Involves Asn 94. The new sugar binding mode of G7 is stabilized in two ways. First, the position of the G7 sugar chain allows formation of a hydrogen bond between the glucose OH-2 group at subsite −4 and the glucose OH-3 group at subsite −5 (Figure 3A). This hydrogen bond is absent in the G9 structure (*12*). Second, the G7 sugar at subsite −3 is stabilized by new hydrogen bonds. The glucose OH-6 group

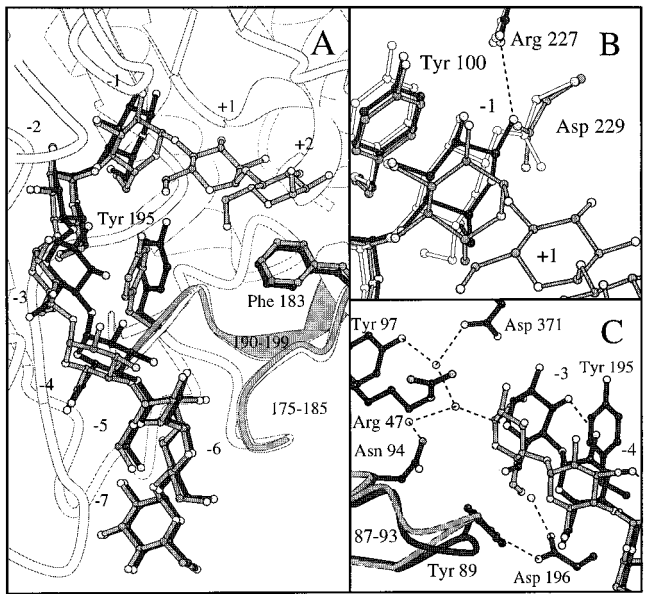

FIGURE 4: (A) Comparison of the G7 structure (sugar and side chains in black, the protein backbone in white) with that of maltononaose complexed to BC251 E257Q/D229N CGTase (G9, gray) (*7*). The G7 sugar conformation at subsite −3 would clash with the G9 protein conformation of Tyr 195, whereas the G7 conformation of Tyr 195 would bump into the G9 sugar conformation at subsite +1. (B) Detail of subsite −1, with the BC251 E257Q CGTase−covalent intermediate structure (*7*) included in white. The position of the G7 glucose ring at subsite −1 most resembles that of the intermediate, with its OH-1 group mimicking the absent Asp 229 Oδ1 atom. The G7 Ala 229 side chain is hidden from view. (C) Detail of the conformational differences at subsite −3. Unconnected white circles indicate water molecules. G7 is stabilized by two water-mediated hydrogen-bonding networks connecting to its O5 and O6 atoms (only one is shown for clarity) and an interglycosidic hydrogen bond to subsite −4. G9 is stabilized by a direct hydrogen bond between the glucose O6 and Asp 196 Oδ1 atoms and a hydrogen bond to Asp 371 (bonds not drawn).

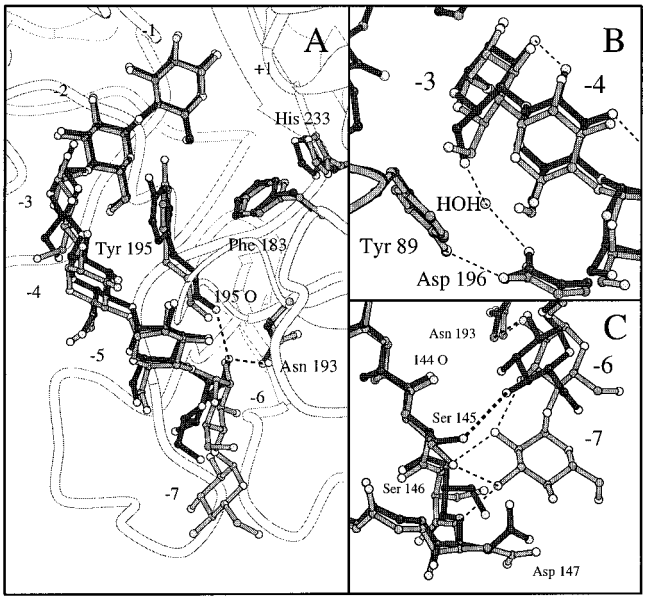

FIGURE 5: (A) Comparison of the G6 structure (sugar in black, protein backbone in white) with the G7 structure (gray). Differences in sugar binding are seen at subsites −3 and −6. His 233 in the G6 conformation narrows subsite +1. (B) Detail of subsite −3, showing the possibility of a water-mediated hydrogen bond between the glucose O6 and Asp 196 Oδ1 in the G6 structure. (C) Detail of subsites −6 and −7, with direct hydrogen bonds in the G6 structures (thick dashed lines) and the G7 structure (thin dashed lines). For water-mediated interactions, see Figure 3.

forms a contact (mediated by two water molecules) to the Asn 94 Oδ atom (not shown). Furthermore, the glucose O5 atom binds to a network of three water molecules that are trapped in a cavity formed by the Asn 94 Nδ, Asp 371 Oδ1, Tyr 97 Oη, His 98 Nε, and Thr 95 backbone O atoms (Figures 3A and 4C). This is the first time that Asn 94 is implicated in (indirect) substrate binding, although it was shown earlier that mutants in Asn 94 affect the catalytic activity of CGTase (*29*).

Tyr 195 in the Maltoheptaose Complex Hinders Binding of a Sugar Acceptor. The absence of bound sugars at the acceptor subsites is a feature that the CGTase G7 complex shares with the CGTase−covalent intermediate complex (*7*). It indicates that the sugars in the experimental setup (maltoheptaose, 4-deoxymaltose) lack sufficient affinity, which is unexpected, since kinetic experiments show that maltose and maltooligosaccharides are high-affinity acceptors for CGTase (*11*). The G7 structure provides a convincing explanation for the absence of acceptor sugars, because the conformation of CGTase itself blocks acceptor binding.

When the CGTase active site in the G7 complex is superimposed on the G9 complex, the flexible loops of residues 190−199 and 175−185 appear to have shifted 0.6 Å toward the +1 acceptor subsite, thereby narrowing this subsite in the G7 complex (Figure 4A). As a result, the centrally located residue Tyr 195 in the 190−199 loop forms close contacts with the superimposed O6 atom (at 2.0 Å) and the C6 atom (at 2.2 Å) of the G9 glucose at subsite +1 (Figure 4A). Thus, loop rearrangements result in a conformation of Tyr 195 in the G7 complex that is incompatible with acceptor binding.

CGTase in the Maltoheptaose Complex Assumes a New Conformational State. Rearrangements of the flexible loops comprising residues 87−93, 175−185, and 190−199 were observed previously for CGTase complexes (*12*). Until now, two conformations of the CGTase active site were known. The first is the conformation of CGTase seen in the unliganded (*18, 19*) and the γ-cyclodextrin-liganded (*12*) complexes, and the second is the conformation of CGTase seen in the G9 complex (*7*). Both conformations were observed to hinder the sugar binding mode of the other state. The unliganded/γ-cyclodextrin protein backbone conformation was observed to hinder G9 binding at subsite −6 by the position of the Tyr 195 carbonyl oxygen atom. The G9 protein conformation was observed to hinder γ-cyclodextrin binding by the position of Tyr 195 at subsite −3 (*12*).

The conformation of CGTase in the G7 complex shows now, surprisingly, a third conformational state, which is incompatible with the previously observed ones. The G7 protein conformation hinders binding of a G9 sugar in subsite +1 (see above) and binding of a G7 sugar to the G9 protein conformation is hindered by a close contact between Tyr 195 and the glucose C3 atom at subsite −3 (2.5 Å) (Figure 4A). In addition, the G7 protein conformation hinders binding of a γ-cyclodextrin at subsite +1 (in a similar fashion as it hinders G9), and binding of a G7 sugar is hindered by the unliganded/γ-cyclodextrin protein conformation of CGTase through a close contact between the Tyr 195 carbonyl oxygen and the glucose O2 atom at subsite −6 (2.2 Å). Thus, CGTase in the G7 complex assumes a new conformational

state of which the protein backbone and the sugar binding mode are incompatible with the other known states.

Maltohexaose Binds Differently from Maltoheptaose at Subsites −3 and −6. The electron density map for the G6 structure, although of lesser quality than that of the G7 structure, shows binding of a maltooligosaccharide from subsites −1 to −6 (Figure 2B). This proves that these subsites can bind sugars independently, without assistance from subsite −7, at which sugar binding is supported by a crystal contact (*10*). The overall conformation of G6 is similar to that of G7 at subsites −1, −2, −4, and −5 but differs at subsites −3 and −6 (Figure 5A). At subsite −3, the glucose of G6 is even further displaced (0.7 Å) out of the Tyr 89−Tyr 195 cleft (Figure 5B), and at subsite −6 the glucose has tilted ∼40° compared to the G7 structure (Figure 5C), forming novel contacts to the Asn 193 Nδ and Ser 145 Oγ atoms (Table 2, Figures 3 and 5C).

Conformational State of CGTase in the G6 Complex Resembles That of the G7 Complex. In the G6 complex, like in that of G7, the 190−199 and 175−185 loops have shifted toward the acceptor cleft, thereby narrowing the +1 acceptor site. However, compared to the G7 complex, both loops have shifted more toward each other, and also the stretch of residues 185−190, which connects both loops, shows a clear displacement. These differences are probably related to the altered crystal packing of the G6 complex near subsite −7 and the Tyr 633/Leu 600 maltose binding site, since both these sites are located close to the flexible loops.

Despite these differences, the G6 complex has the same characteristics that define the G7 complex as a separate conformational state. First, acceptor binding at subsite +1 is hindered, in this case by a 0.8 Å shift of His 233 toward Tyr 195 (Figure 5A). Second, when the G6 sugar ligand is superimposed on the protein conformations of unliganded and G9-complexed CGTase, similar close contacts as for the G7 sugar ligand appear at subsites −6 (2.0 Å), and subsite −3 (2.1 Å), respectively. Thus, the G6 complex of CGTase assumes the same conformational state as the G7 complex.

DISCUSSION

Subsite −1 Prefers To Bind Glucose in an Intermediate-like Position. The complexes of *B. circulans* strain 251 E257A/D229A CGTase with maltoheptaose and maltohexaose show that both sugars bind with their reducing end in subsite −1. The −1 sugar is not fixed in its position by a covalent bond to a glucose at subsite +1 (as in a bound substrate) or to Asp 229 (as in an intermediate). Therefore it is relatively free to assume the most favorable position in this subsite. The fact that the glucose ring takes a covalent intermediate-like position shows that the architecture of subsite −1, in the absence of the catalytic residues Glu 257 and Asp 229, is optimal for intermediate binding, as has been suggested earlier (*7*). In substrate complexes of an α-amylase with an intact nucleophile (Asp 229), van der Waals repulsions between the Asp 229 Oδ1 atom and the C1 atom of a free sugar at subsite −1 prevent the sugar ring from occupying this favorable position (*30*). A similar sterical clash is also observed when the structures of wild-type CGTase and the maltoheptaose complex are superimposed. However, this clash will be absent when the covalent intermediate is formed. Therefore, the structural evidence indicates that, in the α-amylase family, the catalytic site architecture favors the position of the intermediate glucose ring.

Scenario for the CGTase Reaction Cycle Implies an Induced Fit for Sugar Acceptors. The 3D structures of G7 and G6 bound to CGTase represent covalent intermediates with long sugar chains bound at the donor sites but empty acceptor sites. Thereby they complete the X-ray analysis of four different reaction stages of *B. circulans* strain 251 CGTase (Figure 6). The differences between these structures suggest that during the catalytic cycle of CGTase substantial conformational rearrangements take place, for which a possible scenario is presented in Figure 6. This can explain, in part, the high transglycosylation activity of CGTase.

In the first step of substrate binding, CGTase changes from an unliganded (*18*) to a G9 conformation (*7*). The presence of glucoses at subsites +1 and −6 forces Tyr 195 in the direction of subsite −3, where it pushes the substrate toward the 87−93 loop, which in turn changes conformation, together with the 190−199 loop (Figure 6, top right). In earlier work this conformation of CGTase was found to be activated, because in the G9 complex catalytically more proficient conformations are observed for Asn 139 and His 140 at subsite −1 (*12*).

In the next step of covalent intermediate formation, CGTase changes from a G9 (*7*) to a G7 conformation. Cleavage of the scissile bond could stimulate CGTase to relax from its G9 state, in which the 87−93 loop assumes its original orientation, thereby driving the glucose at subsite −3 to its G7 position (Figure 6, bottom right). Molecular dynamics simulations, performed before the G7 structure was known, corroborate such a donor-chain rearrangement at subsite −3 (*31*). The glucose at subsite −3 in turn shifts Tyr 195 to its G7 conformation by close contacts, leading to a narrowing of the +1 acceptor site and expulsion of the leaving group (Figure 6, bottom right).

In the following step, an acceptor has to bind in the narrowed subsite +1 (Figure 1). When a cyclization reaction occurs, CGTase moves from a G7 to a cyclodextrin-liganded conformation (*12*). Departure of the donor chain, which functions as acceptor, from subsite −6 could allow the 190−199 loop to relax and subsite +1 to open (Figure 6, bottom left). When a disproportionation reaction occurs, binding of a free sugar acceptor at subsite +1 would move CGTase again from a G7 to an activated G9 conformation (Figure 6, top right). In contrast, when a hydrolysis reaction occurs, binding of a water molecule as acceptor will probably not induce these conformational rearrangements because it has sufficient space. This suggests an induced-fit mechanism in which binding of a free sugar acceptor specifically activates CGTase, which can explain why CGTase has a much higher transglycosylation (disproportionation) than hydrolysis activity.

Site-Directed Mutagenesis Studies Confirm the Reaction Cycle Model. An important element of this scenario is that close contacts between Tyr 195 and the glucoses at subsites −6, −3, and +1 modulate the reaction cycle. This is substantiated by biochemical data. For instance, CGTase processes maltopentaoses but not maltotetraoses (*32*). Since maltotetraose binds from subsites +2 to −2, and maltopentaoses from +2 to −3 (*18*), this implies that CGTase has a

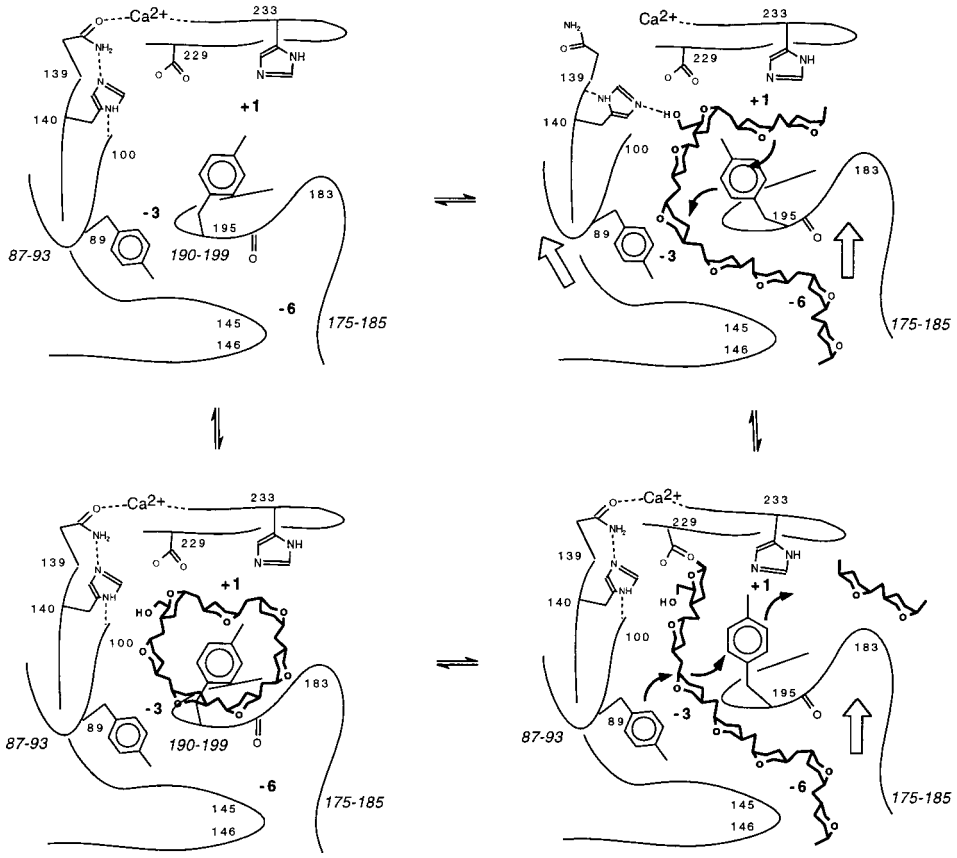

FIGURE 6: Possible scenario for the structural rearrangements during the CGTase reaction cycle. The top left shows a diagram of CGTase in its unliganded state, based on the 2.2 Å BC251 wild-type structure at 120 K (*18*). The top right diagram represents the linear substrate-bound state, based on the 2.1 Å BC251 E257Q/D229N CGTase structure complexed to maltononaose at 120 K (*7*). The bottom left diagram shows the cyclodextrin-bound state, as based on the 1.8 Å BC251 E257Q/D229N CGTase structure complexed to γ-cyclodextrin at 120 K (*12*). On the bottom right, the intermediate state has been reconstructed by a combination of the G7 and G6 structures, and the 1.8 Å BC251 E257Q CGTase covalently bound maltotriose intermediate, at 100 K (*7*). The pictures in clockwise order show a cyclization reaction cycle, and in counterclockwise order a coupling reaction cycle (Figure 1). The hydrolysis and disproportionation cycles (Figure 1) follow top left → top right → bottom right → top right → top left. Small labels indicate amino acid position; labels in italic type indicate flexible loops mentioned in the text. The black arrows represent the series of van der Waals repulsions that in part explain the observed conformational rearrangements (see text). The white arrows represent a simplified view of the CGTase backbone conformation, as compared to its unliganded state.

higher activity when substrates bind at subsite −3, which in our model is important for activation of CGTase.

Investigations of the accceptor specificity of CGTase showed that the OH-2, OH-3, and OH-4 hydroxyl groups of a glucose acceptor are essential for binding but that the OH-6 group adds to the efficiency of acceptor processing (*33*, *34*). This supports the idea that the acceptor C6−OH-6 moiety displaces Tyr 195 from subsite +1 and can thereby induce an activated conformation of CGTase.

Furthermore, site directed mutagenesis data indicate that replacing the amino acid at position 195 in a series of Gly, Phe, Tyr, and Trp results in a proportional increase in k_{cat} (and k_{cat}/K_M) for disproportionation (*11*). Thus, a larger side chain at position 195 enhances the efficiency of the processing of linear sugars. Such a larger side chain is also more likely to have close contacts to sugar ligands at subsites −3 and +1, which in our model lead to activation of CGTase.

At the acceptor subsites, mutagenesis of His 233 at subsite +1 in CGTase results in a 60−30 times decreased k_{cat} for hydrolysis and coupling (cyclodextrin degradation by transglycosylation), and an unchanged K_M for those reactions (*35*). Mutants of residues Phe 259 and Phe 183 at subsite +2 show an increase in affinity for maltose as acceptor (lower K_M) and a decrease in k_{cat} for disproportionation (B. A. van der Veen, unpublished result). These results indicate that the role of these residues is not increasing the acceptor affinity, in which case mutants would have shown higher K_M values, but increasing the catalytic efficiency (k_{cat}), which is consistent with our model in which acceptor binding activates the reaction cycle.

G7 and G6 Binding at the Donor Subsites Reveals α/β-Cyclodextrin Specificity. Whereas acceptor binding determines the high transglycosylation activity of CGTase, donor sugar binding is important for the cyclodextrin size specificity. These latter subsites determine the size of the linear substrate that is bound at the start of the reaction and thus also the size of the product. Therefore, the G6 and G7 complexes should give insight into the determinants for α- and β-cyclodextrin specificity, respectively.

Since structural differences between G6 and G7 binding occur at subsites −3, −6, and −7 (Figure 5), changes at these subsites that favor one binding mode over the other will result in changes in α/β-cyclodextrin size specificity. At subsite −7, a mutation S146P that blocks sugar binding shows a specific decrease in the initial rate of β-cyclodextrin formation (*13*). Also the Δ(145−151) deletion mutant of *B. circulans* strain 8 CGTase, which removes most interactions at subsite −7, shows a reduced production of β-cyclodextrin

(*16*). At subsite −3, mutants in Tyr 89 and Asp 196 that stimulate binding of substrate in an orientation that resembles the G6 binding mode show an enhanced rate of α-cyclodextrin formation (*13*, *36*). On the other hand, mutation of Asn 94, a residue that specifically stabilizes the G7 binding mode, results in a decreased *β*-cyclodextrin production (*29*). Of subsite −6, no mutagenesis studies are known. These results support the view that differences in the binding mode of G6 and G7 reveal determinants of α/*β*-cyclodextrin size specificity. The conclusion that these determinants are located at subsites −3, −6, and −7 is in agreement with comparisons of natural CGTases with different size specificities that show the highest sequence variation in subsites −3 and −7 (*12*).

CONCLUSIONS

Maltoheptaose (G7) and maltohexaose (G6) bind to E257A/D229A CGTase at the donor subsites and leave the acceptor sites empty. At subsite −1, these sugars occupy a position that is similar to that of the covalent intermediate, suggesting that this is the favored binding mode in that subsite. At the other donor subsites, the sugar residues assume a conformation which is different from that in previously determined CGTase complexes. This induces a conformation in CGTase that hinders sugar binding in the acceptor sites. An analysis of the CGTase reaction cycle based on the known structures of reaction stages suggests that binding of a sugar acceptor to the G7 and G6 complexes will induce structural rearrangements that activate catalysis. By such an induced-fit mechanism, the preference of CGTase for transglycosylation rather than hydrolysis can be explained.

Since CGTase will form α-cyclodextrin from G6 and *β*-cyclodextrin from G7, differences between the binding of G7 and G6 give insight into the factors that determine cyclodextrin product size specificity. The conformations of G6 and G7 are most different at subsites −3, −6, and −7, and mutagenesis studies confirm that favoring one sugar binding mode over the other at these subsites alters the cyclodextrin size specificity in a predictable fashion.

ACKNOWLEDGMENT

We thank Harm Mulder for his work on the E257A/D229A CGTase mutant, Dr. Paul Tucker for assistance with data collection, and Professor Jan Drenth for critically reading the manuscript.

REFERENCES

1. Henrissat, B., and Davies, G. (1997) *Curr. Opin. Struct. Biol. 7*, 637−644.
2. Svensson, B. (1994) *Plant Mol. Biol. 25*, 141−157.
3. Janecek, S. (1997) *Prog. Biophys. Mol. Biol. 67*, 67−97.
4. Kuriki, T., and Imanaka, T. (1999) *J. Biosci. Bioeng. 87*, 557−565.
5. Jespersen, H. M., MacGregor, E. A., Sierks, M. R., and Svensson, B. (1991) *Biochem. J. 280*, 51−55.
6. McCarter, J. D., and Withers, S. G. (1994) *Curr. Opin. Struct. Biol. 4*, 885−892.
7. Uitdehaag, J. C. M., Mosi, R., Kalk, K. H., van der Veen, B. A., Dijkhuizen, L., Withers, S. G., and Dijkstra, B. W. (1999) *Nat. Struct. Biol. 6*, 432−436.
8. Crabb, W. D., and Mitchinson, C. (1997) *Trends Biotechnol. 15*, 349−352.
9. Pedersen, S., Dijkhuizen, L., Dijkstra, B. W., Jensen, B. F., and Jørgensen, S. T. (1995) *CHEMTECH*, 19−25.
10. Strokopytov, B., Knegtel, R. M. A., Penninga, D., Rozeboom, H. J., Kalk, K. H., Dijkhuizen, L., and Dijkstra, B. W. (1996) *Biochemistry 35*, 4241−4249.
11. van der Veen, B. A., van Alebeek, G.-J. W. M., Uitdehaag, J. C. M., Dijkstra, B. W., and Dijkhuizen, L. (2000) *Eur. J. Biochem. 267*, *658*-665.
12. Uitdehaag, J. C. M., Kalk, K. H., van der Veen, B. A., Dijkhuizen, L., and Dijkstra, B. W. (1999) *J. Biol. Chem. 274*, 34868−34876.
13. van der Veen, B. A., Uitdehaag, J. C. M., Penninga, D., van Alebeek, G.-J. W. M., Smith, L. M., Dijkstra, B. W., and Dijkhuizen, L. (2000) *J. Mol. Biol. 296*, *1027−1038.*
14. Terada, Y., Yanase, M., Takata, H., Takaha, T., and Okada, S. (1997) *J. Biol. Chem. 272*, 15729−15733.
15. Tonkova, A. (1998) *Enzyme Microb. Technol. 22*, 678−686.
16. Parsiegla, G., Schmidt, A. K., and Schulz, G. E. (1998) *Eur. J. Biochem. 255*, 710−717.
17. Sin, K.-A., Nakamura, A., Masaki, H., Matsuura, Y., and Uozumi, T. (1994) *J. Biotechnol. 32*, 283−288.
18. Knegtel, R. M. A., Strokopytov, B., Penninga, D., Faber, O. G., Rozeboom, H. J., Kalk, K. H., Dijkhuizen, L., and Dijkstra, B. W. (1995) *J. Biol. Chem. 270*, 29256−29264.
19. Lawson, C. L., van Montfort, R., Strokopytov, B., Rozeboom, H. J., Kalk, K. H., de Vries, G. E., Penninga, D., Dijkhuizen, L., and Dijkstra, B. W. (1994) *J. Mol. Biol. 236*, 590−600.
20. Mosi, R., He, S., Uitdehaag, J., Dijkstra, B. W., and Withers, S. G. (1997) *Biochemistry 36*, 9927−9934.
21. Otwinowski, Z. (1993) in *Data Collection and Processing* (Sawyer, L., Isaacs, N., and Bailey, S., Eds.) pp 56−62, SERC Laboratory, Daresbury, U.K.
22. Tronrud, D. E., Ten Eyck, L. F., and Matthews, B. W. (1987) *Acta Crystallogr. A43*, 489−501.
23. Read, R. J. (1986) *Acta Crystallogr. A42*, 140−149.
24. Vellieux, F. M. D., and Dijkstra, B. W. (1997) *J. Appl. Crystallogr. 30*, 396−399.
25. Jones, T. A., Zou, J. Y., Cowan, S. W., and Kjeldgaard, M. (1991) *Acta Crystallogr. A47*, 110−119.
26. Jeffrey, G. A. (1990) *Acta Crystallogr. B46*, 89−103.
27. Hooft, R. W. W., Vriend, G., Sander, C., and Abola, E. E. (1996) *Nature 381*, 272−272.
28. Navaza, J., and Saludjian, P. (1997) in *Methods in Enzymology* (Carter, C. W., Jr., and Sweet, R. M., Eds.) pp 581−594, Academic Press, London.
29. Kim, Y. H., Bae, K. H., Kim, T. J., Park, K. H., Lee, H. S., and Byun, S. M. (1997) *Biochem. Mol. Biol. Int. 41*, 227−234.
30. Yoshioka, Y., Hasegawa, K., Matsuura, Y., Katsube, Y., and Kubota, M. (1997) *J. Mol. Biol. 271*, 619−628.
31. Uitdehaag, J. C. M., Elber, R., van der Veen, B. A., Dijkhuizen, L., and Dijkstra, B. W. (2000) (in preparation).
32. Bender, H. (1985) *Carbohydr. Res. 135*, 291−302.
33. Kitahata, S., Okada, S., and Fukui, T. (1978) *Agric. Biol. Chem. 42*, 2369−2374.
34. Nakamura, A., Haga, K., and Yamane, K. (1994) *FEBS Lett. 337*, 66−70.
35. Nakamura, A., Haga, K., and Yamane, K. (1993) *Biochemistry 32*, 6624−6631.
36. Wind, R. D., Uitdehaag, J. C. M., Buitelaar, R. M., Dijkstra, B. W., and Dijkhuizen, L. (1998) *J. Biol. Chem. 273*, 5771−5779.
37. Esnouf, R. M. (1999) *Acta Crystallogr. D55*, 938−940.

BI000340X